J. of Thermal Science Vol.9, No.2

Effect of Eccentricity and Radius Ratio on Fluid Flow and Heat Transfer Inside an Eccentric Semicircular Enclosure

Prodip Kumar Das Shohel Mahmud
Department of Mechanical Engineering, Bangladesh University of Engineering & Technology (BUET), Dhaka-1000, Bangladesh

The problem of laminar natural convective heat transfer inside an eccentric semicircular enclosure of different radius ratio and eccentricity is investigated numerically. At the same time, combined effect of the radius ratio and eccentricity on fluid flow is also observed with isothermal upper and lower surface. Here laminar, steady natural convection heat transfer are predicted for radius ratio R^*=1.75, 2.0, 2.25, 2.5. Simulation was carried out for a range of eccentricity, ε=0.0 to 0.6. Governing equations are solved using finite volume method with a body fitted grid with collocated variable arrangement for a range of Grashof number 10^1-10^7 based on R_0. Results are presented in the form of constant stream function, isothermal lines, local Nusselt number and average Nusselt number at different angular position. Eccentricity has little dominance on heat transfer rate. But significant effect of eccentricity is observed on flow field. Radius ratio has significant effect on natural convection heat transfer as well as on flow field. At higher eccentricity, bi-cellular flow is observed with one crescent-shape vortex at narrower cross section. This crescent shaped vortex is broken down into two cells with the increase of radius ratio that means transition Grashof number for bi-cellular flow to tri-cellular flow is decreased with the increase of radius ratio. Eccentricity also has the same effect on flow field. Eccentricity has little effect on heat transfer but with the increase of radius ratio, average heat transfer rate increases.

Keywords: eccentricity, eccentric enclosure, Nusselt number, radius ratio

Introduction

Natural convection heat transfer has gained considerable attention because of its numerous applications in the areas of energy conservation, cooling of electrical and electronic components, design of solar collectors, heat exchangers, and many others. Heat transfer inside annular space, air-filled cavity or annular sector has wide application in many engineering problems. In our earlier work[1,2], we have shown the effect of eccentricity on heat transfer and flow field for radius ratio R^*=2.0 for different eccentricity (ε=0.2, 0.4, 0.6). But here we are trying to find out the combined effect of eccentricity and radius ratio on heat transfer and fluid flow in a semicircular enclosure. Kuhen & Goldstein[6-8] presented reviews of the available literature and experimental results in concentric and eccentric horizontal cylindrical annuli. Glakpe et al.[9] examined the effect of mixed boundary condition on heat transfer in eccentric enclosures. Yang et. al.[10] investigated steady laminar natural convection in a maximum eccentric (ε=1.0) horizontal annulus with different diameter ratios and three eccentric position. Some other numerical works presented[11,12] heat transfer inside eccentric cylindrical annuli. In this paper, laminar steady natural convection heat transfer has been studied for four different radius ratio with different eccentricity. Rate of heat transfer in terms of local and global Nusselt numbers are presented for different angular positions of inner semicircular surface and Grashof number respectively. Flow and thermal fields are analyzed by parametric presentation of streamlines and isothermal lines.

Problem Formulation

Consider a fluid enclosed in a space bounded by two semicircular surface of radius R_o and R_i as shown in Fig.1. The surface of the semicircular surface are maintained at constant uniform temperatures T_i and T_o,

Received 2000.

Nomenclature

g	gravity vector	T_i	inner wall temperature
Gr	Grashof number, $(\rho^2 g\beta\Delta TR^3_o/\mu^2)$	T_0	outer wall temperature
h	Convective heat transfer coeff.	T_α	fluid temperature
K_f	thermal conductivity of fluid	T_{ref}	reference temperature
Nu_{av}	average Nusselt number	Q	heat transfer
Nu_L	local Nusselt number, $(h\ R_o/K_f)$		**Greek symbol**
p	pressure	β	Thermal expansion coeff.
R_i	radius of inner semicircle	ε	eccentricity
R_o	radius of outer semicircle	μ	dynamic viscosity
R^*	radius ratio (R_0/R_1)	ρ	mass density
		θ	angular position

where $T_i > T_o$. Two horizontal surfaces that connect outer and inner semicircular surface are considered adiabatic. In present investigation, we take the advantage of finite volume method to generate body fitted grid with collocated variable arrangement. The integral forms of governing equations are as follows:

$$\int_S \rho \boldsymbol{v}\cdot\boldsymbol{n}\, ds=0 \tag{1}$$

$$\int_S \rho u_i \boldsymbol{v}\cdot\boldsymbol{n}\, ds=\int_S \mu\, grad u_i\cdot\boldsymbol{n}\, ds-\int_S p\boldsymbol{i}_i\cdot\boldsymbol{n}\, ds+\int_V \rho b_i dv \tag{2}$$

$$\int_S \rho u_j \boldsymbol{v}\cdot\boldsymbol{n}\, ds=\int_S \mu\, grad u_j\cdot\boldsymbol{n}\, ds-\int_S p\boldsymbol{i}_j\cdot\boldsymbol{n}\, ds+\int_V \rho b_j dv \tag{3}$$

$$\int_S \rho T\boldsymbol{v}\cdot\boldsymbol{n}\, ds=\int_S k\ grad T\cdot\boldsymbol{n} ds \tag{4}$$

Here b_i is the body force in the i th Cartesian direction. In cases considered here, the only body force is the buoyancy force, which is implemented by applying the Boussinesq approximation:

$$\rho\, b_i = \rho_0\ g_i\ \beta\ (T - T_0) \tag{5}$$

Where g_i is the i th component of the gravity acceleration vector, T_0 is the reference temperature and ρ_0 is the density at T_0. Equation (1) - (4) can be written in a generalized form:

$$\int_S \rho\phi\boldsymbol{v}\cdot\boldsymbol{n} ds = \int_S \Gamma grad\phi\cdot\boldsymbol{n} ds + \int_V q_\phi dv \tag{6}$$

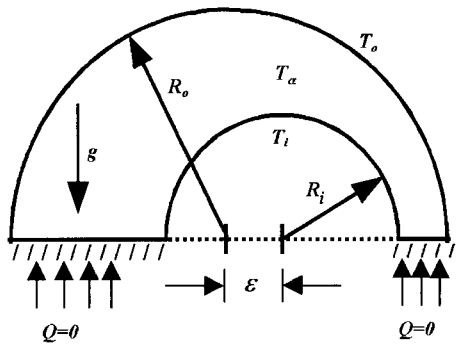

Fig.1 Schematic diagram of problem under consideration

Previous equations are discretized using control-volume based finite volume method with collocated variable arrangement. Solution procedures with detail algorithm are available in references [4,5]. Schematic diagram of the computational domain under consideration is shown in Fig.1, with various geometrical parameters. Radius ratio is defined as the ratio between the outer radius and inner radius.

Results and Discussions

Three grid sizes (30×16, 60×32, and 120×64) were chosen to carry out present simulation. Results are presented for fine grid (120×64). For a particular eccentricity, Grashof number was varied by changing dynamic viscosity keeping other fluid and geometric variables constant. Iteration was stopped when difference between two consecutive variable values for all variables fall below 10^{-5}. For further stabilization of numerical procedure, relaxation factor was chosen between 0.1-0.7.

Local heat transfer

Local Nusselt number distribution along the surface of lower semicircular surface is shown in Fig.2 for $Gr=10^2$ & 10^5. At $Gr=10^2$, heat transfer is almost invariant along the periphery of the lower semicircular surface except two corners for ε=0.0 shown in Fig. 2(a). With the increase of eccentricity, heat transfer rate is higher for angular position (θ) between 0^0 to 100^0, between 100^0 to 180^0 heat transfer rate is lower. For each radius ratio, similar profiles of heat transfer pattern are observed having higher rate of heat transfer at higher R* shown in Fig. 3(a). Interesting scenario is observed at $Gr=10^5$, periodic heat transfer rate (with respect to angular position) is observed for different radius ratio. This is happened due to symmetric multi-cellular flow inside the enclosure. For lower radius ratio, symmetrical nature of multi-cellular flow corrupts causing breakdown the periodic nature (with respect to angular position) of heat transfer at $Gr=10^6$. Fig.4 shows the Nusselt number distribution at different Grashof number for constant radius ratio and eccentricity.

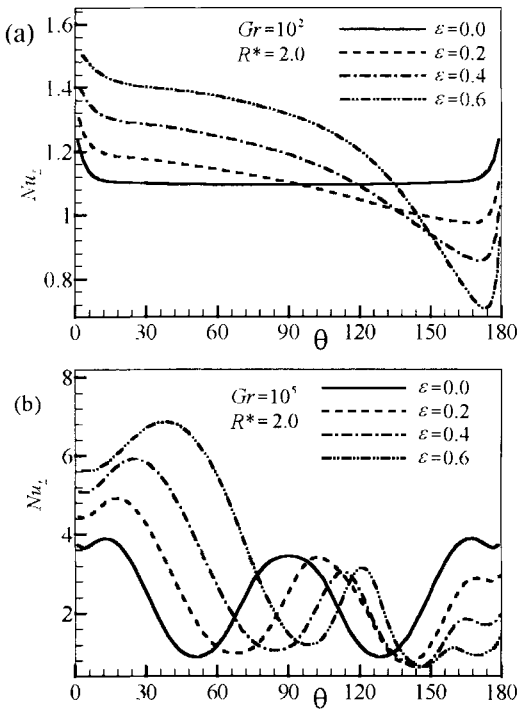

Fig.2 Variation of local Nusselt number along lower semicircular surface for different eccentricity, θ is measured from left to right (clockwise) over the lower semicircle

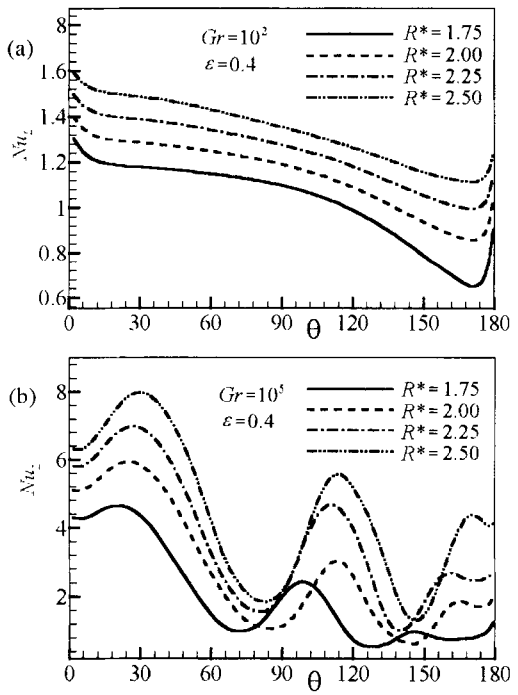

Fig.3 Variation of local Nusselt number for different radius ratio

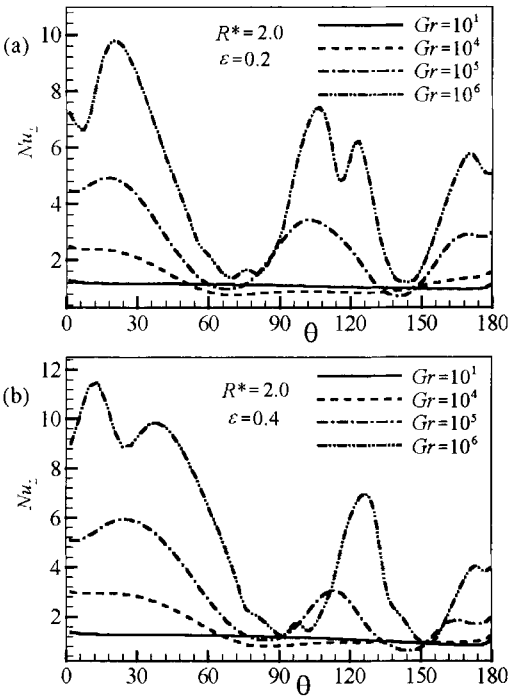

Fig.4 Local Nusselt number distribution at fixed R^* and ε for different Grashof number

Average heat transfer

The effect of radius ratio on average heat transfer is shown in Fig.5 (a). At lower Grashof number the

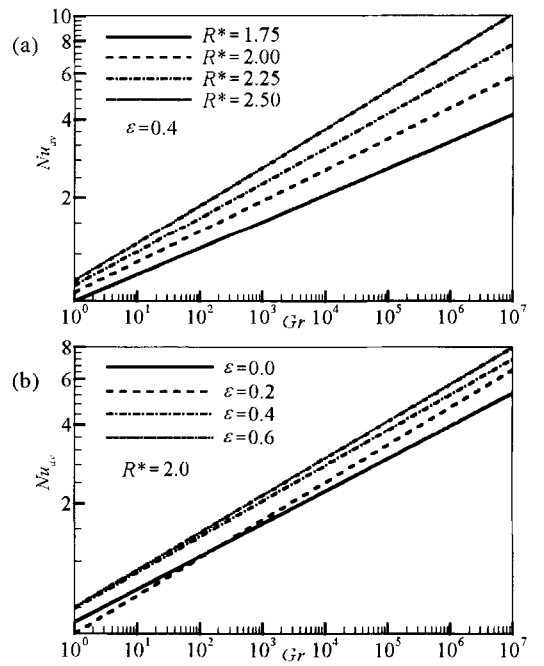

Fig.5 Variation of average Nusselt number with Grashof numbers for different radius ratio and eccentricity

effect of radius ratio is very small but at higher Grashof number the effect is significant. At higher radius ratio heat transfer rate is higher than the lower one. Eccentricity has little effect on average heat transfer rate at lower Grashof number shown in Fig. 5(b) but at higher Grashof number heat transfer is increased slightly with eccentricity.

Flow field

Figs. 6-9 show the constant streamfunction contours at six different Grashof number for R^*=2.0 & ε=0.2, R^*=2.0 & ε=0.4, R^*=2.5 & ε=0.2 and R^*=2.5 & ε=0.4. At lower radius ratio with lower eccentricity, bi-cellular flow is observed at $Gr=10^2$ with one crescent-shape vortex at narrower cross section. Bi-cellular flow turns into tri-cellular between $Gr=10^4$–3×10^4. At $Gr=4\times10^4$, tri-cellular flow turns into multi-cellular flow and finally goes into turbulence at $Gr=10^7$. Multi- cellular flow with three small vortices at narrower cross section and a large vortex at larger cross section are observed at higher eccentricity of same radius ratio at higher Grashof number. Instability in hydrodynamic boundary layer at narrower cross section breaks the crescent-shape vortex into three separate small circulation zones. The distorted streamlines at $Gr=10^7$ indicate transition to turbulence. Interesting pattern is observed here that the multi-cellular pattern is changed into bi-cellular pattern again. Similar pattern observed at

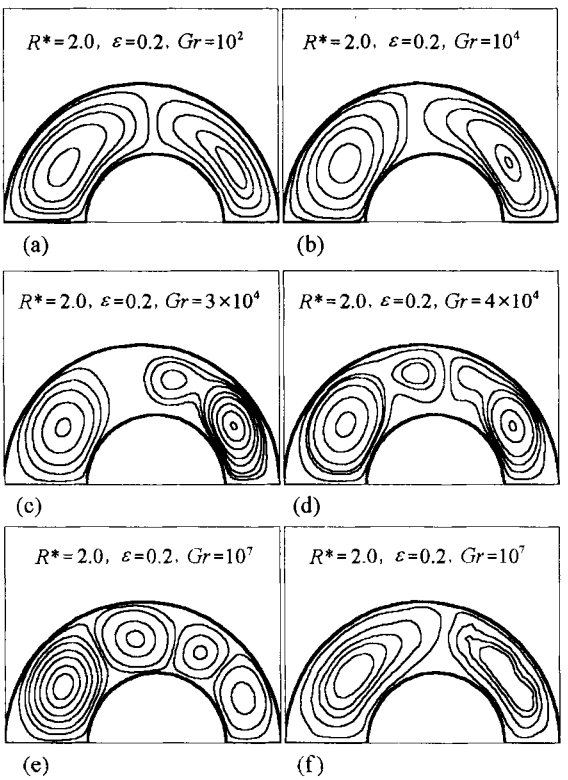

Fig.6 Streamlines at different Grashof number for R^*=2.0 & ε=0.2

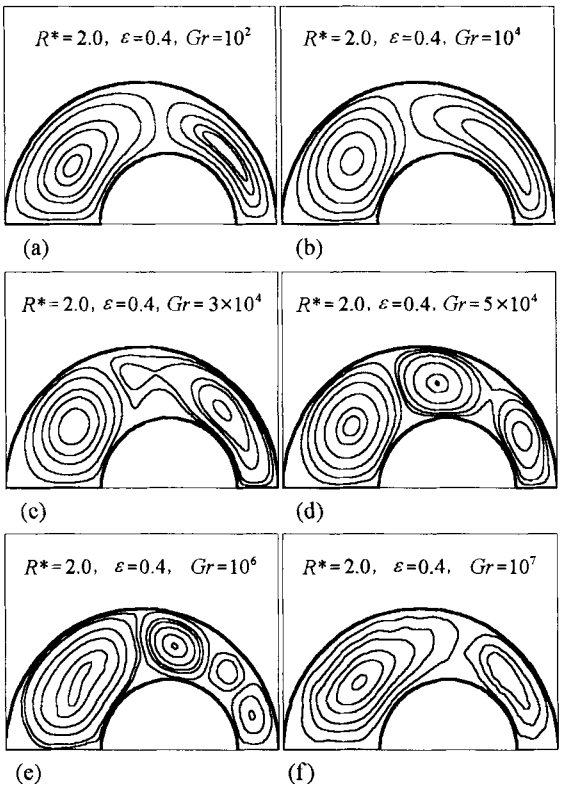

Fig.7 Streamlines at different Grashof number for R^*=2.0 & ε=0.4

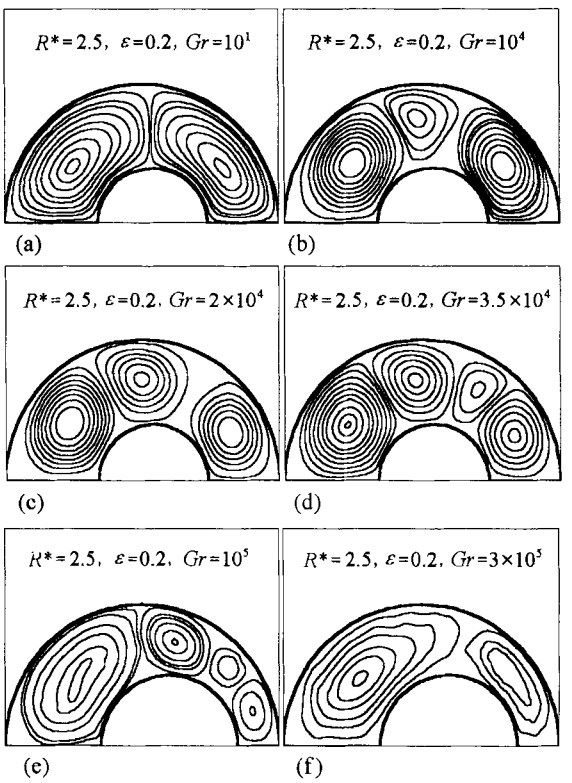

Fig.8 Streamlines at different Grashof number for R^*=2.5 & ε=0.2

higher radius ratio for different eccentricity. At lower radius ratio and eccentricity tri-cellular pattern observed at $Gr=3\times10^4$ and multi-cellular pattern found at $Gr=4\times10^4$–10^5. But at higher radius ratio and eccentricity these two patterns are found at lower Grashof number Fig.9(b) and Fig.9(d) shows the pattern of tri-cellular and multi-cellular respectively. Also transition to turbulence happened at lower Grashof number but for higher radius ratio with lower eccentricity this value is lower than the value of higher eccentricity. At $R^*=2.5$ & $\varepsilon=0.2$ critical Grashof number is near to 3×10^5.

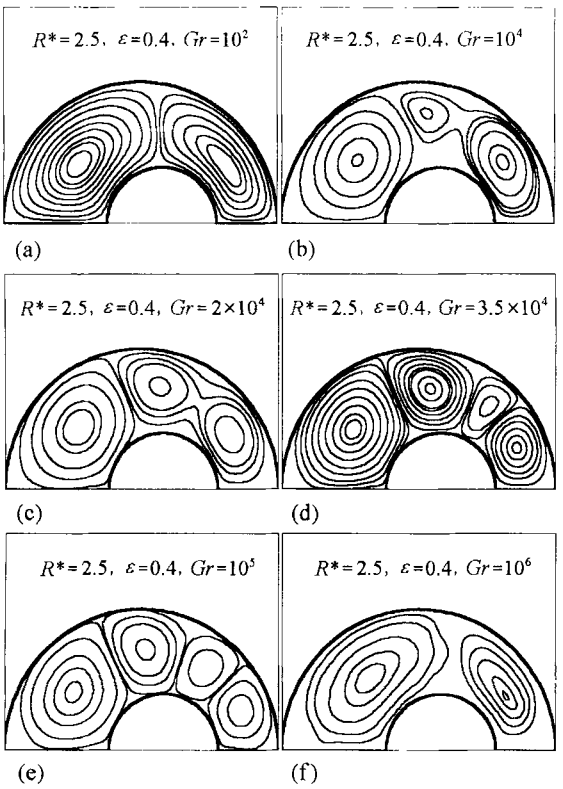

Fig.9 Streamlines at different Grashof number for $R^*=2.5$ & $\varepsilon=0.4$

Thermal field

Thermal field are presented by isothermal lines in Figs. 10-13 for $R^*=2.0$ & $R^*=2.5$. At $Gr=10^2$, buoyancy effect is almost negligible. Isothermal lines are semicircular in shape showing uniform temperature gradient normal to the lower semicircular surface at lower Grashof number. Isothermal lines are concentrated near the left most corner of the inner semicircular surface showing higher temperature gradient at Grashof number 10^4. Other parts of the enclosure show uniform distribution of isothermal lines. Transition to tricellular flow changes the isotherm pattern at $Gr=10^4$. Clearly three spots of high nearwall temperature gradient normal to the inner semicircular

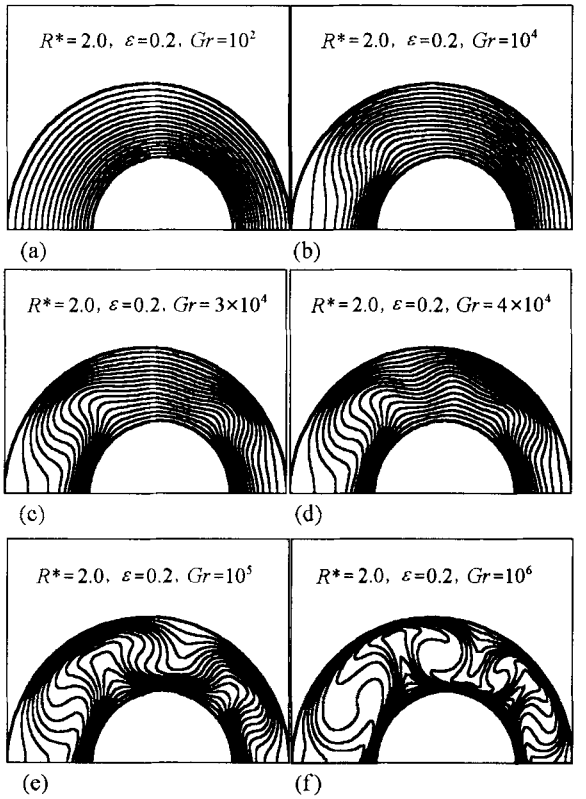

Fig.10 Isothermal lines at different Grashof number for $R^*=2.0$ & $\varepsilon=0.2$

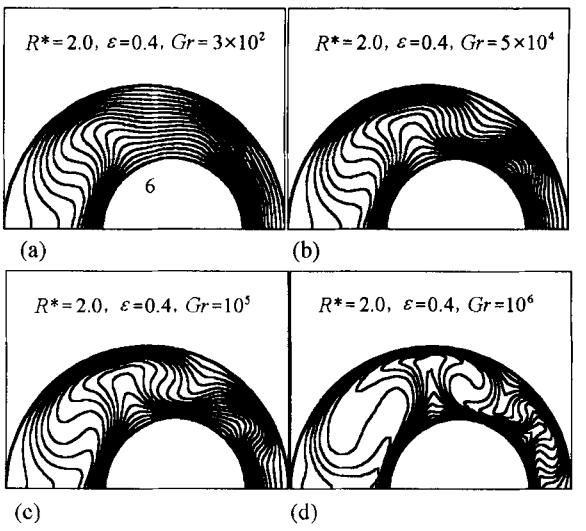

Fig.11 Isothermal lines at different Grashof number for $R^*=2.0$ & $\varepsilon=0.4$

surface are observed at $Gr=10^5$ (Fig.10e) .Heat transfer rates are higher at these spots. Similar pattern is observed at $Gr=5\times10^4$ (Fig.11b) for same radius ratio having higher eccentricity. But temperature gradient is higher than previous case and the hot plume is

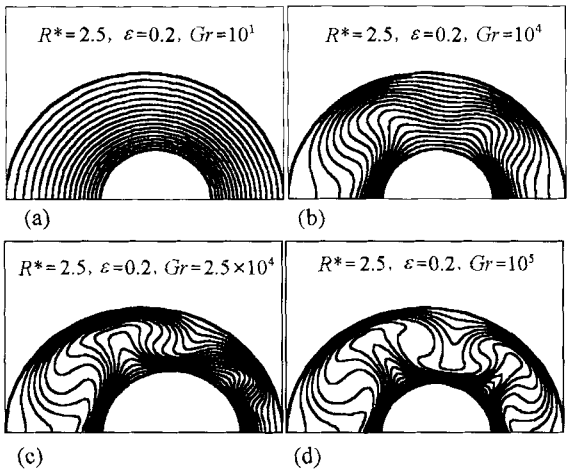

Fig.12 Isothermal lines at different Grashof numbers for R^*=2.5 & ε=0.2

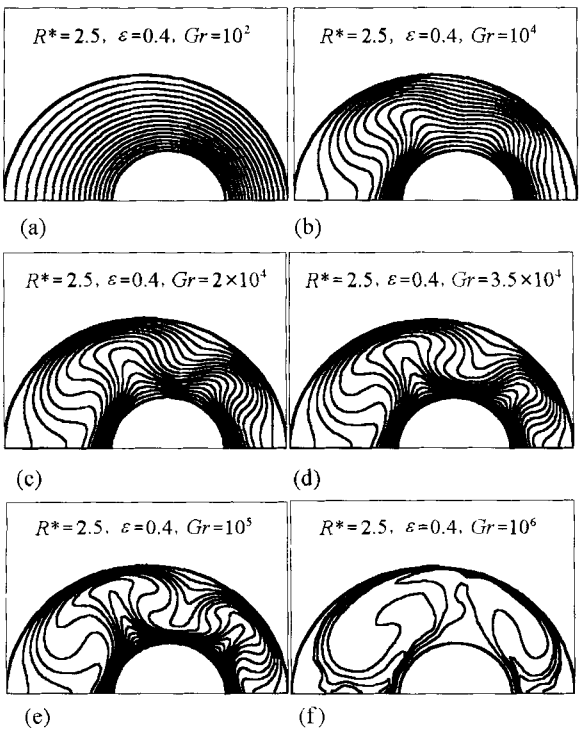

Fig.13 Isothermal lines at different Grashof numbers for R^*=2.5 & ε=0.4

developed fully here and a portion of isotherms begins to swirl shown in Fig.10(f), 11(d), 12(d), and 13(e). This is due to the presence of multi-cellular flow pattern. The distorted isothermal lines at Gr=10^6 indicate transition to turbulence.

Conclusions

Effect of radius ratio & eccentricity on natural convection heat transfer and buoyancy-induced flow inside a semicircular eccentric enclosure is investigated numerically. Radius ratio affects both local heat transfer pattern and flow field. Eccentricity changes the true periodic pattern of local heat transfer of concentric enclosure. Radius ratio has significant influence on average heat transfer rate whereas eccentricity has a little. Crescent-shape vortex is observed at smaller cross section at lower Grashof number, which distorted into bicellular and then into multicellular pattern at higher Grashof number for lower radius ratio. But at higher radius ratio with lower eccentricity similar behavior is observed at lower Grashof number. But the vortex of larger cross sectional area remains almost unchanged with the increase of Grashof number. With the increase of radius ratio critical Grashof number decreases and with the increase of eccentricity the value of critical Grashof number increases.

References

[1] P. K. Das, S. Mahmud, "Buoyancy induced flow and heat transfer inside a semicircular eccentric enclosure," Proc. of 3rd ICFMHT'99, Dhaka, Bangladesh, pp.270-275, (1999).

[2] P. K. Das, S. Mahmud, "Effect of radius ratio on natural convection heat transfer inside an eccentric semicircular enclosure," Proc. of the Sixth Annual Paper Meeting and International Conference, The Institute of Engineers, Bangladesh, pp. 46-53, (2000).

[3] J. C. Chai, S. V. Patankar, "Laminar natural convection in internally finned horizontal annuli," Numerical Heat Transfer, **24**, (1993).

[4] J. Ferziger, M. Peric, "Computational methods for fluid dynamics," Springer Verlag, Berlin Heidelberg, (1996)

[5] S. V. Patankar, "Numerical heat transfer and fluid flow," McGraw-Hill, New York, (1980).

[6] T. H. Kuhen, R. J. Goldstein, "An experimental and theoretical study of natural convection in the annulus between horizontal concentric cylinders," J. Fluid Mech., **74**, (1976).

[7] T. H. Kuhen, R. J. Goldstein, "An experimental study of natural convection heat transfer in concentric and eccentric horizontal cylindrical annuli," J. Heat Transfer, **100**, (1978).

[8] T. H. Kuhen, R. J. Goldstein, "A parametric study of Prandtl number and diameter ratio effects on natural convection heat transfer in horizontal cylindrical annulus," J. Heat Transfer, **102**, (1980).

[9] E. K. Glakpe, C. B. Watkins, "Effect of mixed boundary conditions on natural convection in concentric and eccentric annular enclosure," AIAA Paper, (1987).

[10] Z. Yang, J. He, "A study of natural convection heat transfer in a maximum eccentric horizontal annulus," Proc. of 11th IHTC, **3**, (1998).

[11] C. H. Cho, K. S. Chang and K. H. Park, "Numerical simulation of natural convection in concentric and eccentric horizontal annuli," ASME, J. of Heat Transfer, **104**, (1982).

[12] J. Prusa, L. S. Yao, "Natural convection heat transfer between eccentric horizontal cylinders," ASME, J. of Heat Transfer, **105**, (1983).